
Power Law Rheology of Folded Protein Hydrogels

Anders Aufderhorst-Roberts^{1,2} Sophie Cussons^{3,4} David J. Brockwell,^{3,4} Lorna Dougan^{2,3*}

**1 Centre for Materials Physics, Department of Physics,
University of Durham, Durham, DH1 3LE, UK**

**2 School of Physics and Astronomy,
University of Leeds, Leeds, LS2 9JT, UK**

**3 Astbury Centre for Structural Molecular Biology,
University of Leeds, Leeds, UK**

**4 School of Molecular and Cellular Biology, Faculty of Biological Sciences,
University of Leeds, Leeds, LS2 9JT, UK**

*l.dougan@leeds.ac.uk.

Abstract

Folded protein hydrogels are prime candidates as tuneable biomaterials but it is unclear to what extent their mechanical properties have mesoscopic, as opposed to molecular origins. To address this, we probe hydrogels of the muscle-derived protein *I27*₅, using a multimodal rheology approach. Across multiple protocols, the hydrogels consistently exhibit power-law viscoelasticity in the linear viscoelastic regime with an exponent $\beta = 0.03$, suggesting a dense fractal meso-structure, with predicted fractal dimension $d_f = 2.48$. In the nonlinear viscoelastic regime, the hydrogel undergoes stiffening and energy dissipation, indicating simultaneous alignment and unfolding of the folded proteins. Remarkably, this behaviour is highly reversible, as the value of β , d_f and the viscoelastic moduli return to their equilibrium value, even after multiple cycles of deformation. This highlights a previously unrevealed diversity of viscoelastic properties that originate on the mesoscopic scale. These considerations are likely to be key to controlling the viscoelasticity of folded protein hydrogels.

Introduction

Hydrogels are hydrated three-dimensional networks with significant potential in applications that involve the repair and replacement of biological tissue. [1] A desired aspect of their design is that they mimic the material properties of the tissue that they are designed to replace. The ability to emulate biomechanical properties such as toughness, strain-stiffening and mechanical memory is therefore an important scientific challenge, particularly for applications involving cell growth and proliferation. [2] The design challenges to recreate these properties are significant since materials must be sufficiently soft to allow cell proliferation and sufficiently stiff to protect the material from large and sudden deformations. [3] In living matter, this trade-off is enabled by the unique mechanical properties of biopolymers and their ability to increase their stiffness when deformed and to accommodate large strains through force induced unfolding. [4] Discovering approaches that can recreate these properties in synthetic materials remains highly challenging.

An increasingly promising approach to address this challenge is to construct chemically crosslinked hydrogels from folded proteins. [5–8] In nature, protein domains have precise structures which change their conformation under precise chemical and mechanical conditions. When engineered as polyproteins, their relatively small molecular size ($\sim 10\text{--}100\text{kDa}$) distinguishes them from conventional biopolymers, however when crosslinked into hydrogels, polyproteins exhibit impressive mechanical properties such as high elasticity [9] and resilience [6]. These properties can be controlled through chemical stimuli [10,11], which suggests they may be used in applications involving shape change and shape programming. [7,12,13] Their use is further advantageous since the molecular mechanics of folded protein domains have been extensively interrogated using force spectroscopy [14–16] and can be correlated to bulk viscoelasticity. [17,18]

All hydrogels are intrinsically cross-length scale materials; however, most studies of folded protein hydrogels have focused only on the molecular scale mechanics of the protein and on the bulk properties of the resulting hydrogel. Recent findings from our group have shown that structural parameters at the meso-scale may also be of importance. These include the intermediate structural hierarchy including cross-linking, [19–21] which can be used to modulate the network growth and the fractal dimensions and force distribution of percolating clusters. [22,23] This rich hierarchy of structural properties indicates that polyprotein hydrogels are likely to exhibit complex viscoelastic behaviours, which should manifest themselves in their mechanical response. Relating this mechanical response to the underlying structure can be achieved through shear rheology, since the time-dependent viscoelasticity of the hydrogel directly reflects the length scale of the hydrogel structure. [24] However, most studies of polyprotein hydrogels have instead used dynamic mechanical analysis, (DMA) which is instructive for quantifying bulk elastic properties such as toughness and fracture stress but less effective in quantifying viscoelastic and structural properties. In comparison to shear rheology, DMA may also induce volumetric sample changes at high strains, which may frustrate accurate interpretation of the data. [25] However, a multi-modal rheological characterisation of polyprotein hydrogels that relates time-dependent viscoelasticity to underlying structure has yet to be carried out.

In this study, we seek to bridge the gap between the molecular and bulk mechanics of folded protein hydrogels, using shear rheological tests to probe their meso-scale mechanics. We construct hydrogels using $I27_5$ polyproteins, so called because they comprise five concatenated $I27$ immunoglobulin domains of the muscle protein titin. Titin is an elastomeric component of the sarcomeres of striated muscle, where its $I27$ domains are able to unfold and refold to prevent overstretching. [26] Reflecting this biological role, the $I27$ protein possesses mechanical stability whereas other domains in titin extend with low resistance. It also possesses a high degree of mechanical reversibility, [27,28] as well as being suitable for crosslinking into a hydrogel using photochemical approaches. [29] This makes it a putative robust and tough polyprotein and an excellent candidate for this study. We probe $I27_5$ hydrogels through frequency-dependent small amplitude oscillatory shear, stress relaxation and strain ramp experiments, to probe the viscoelastic properties at a range of timescales and within different regimes of deformation. By combining these different modes of rheology, we present a comprehensive rheological analysis of $I27_5$ hydrogels that infers their meso-scale structure, reveals how this structure relates to viscoelasticity and explores how this viscoelasticity determines the nonlinear and fracture mechanics of the hydrogel.

Methods

Polyprotein Purification

The assembly of $I27_5$ polyproteins was performed using a PCR-based Golden Gate protocol with a modified pET14b, with all original BsaI sites removed, as the destination expression vector. [30] After verification of the DNA sequence, the resulting vector was transformed into BLR (DE3) pLysS *E. coli* cells. 2 ml LB starter culture was used to inoculate 0.5 L autoinduction medium. 10×0.5 L cell cultures were incubated at 28°C, 200 rpm for 24 h, for protein expression and then harvested and lysed. The protein was loaded on to 2×5 ml HisTrap FF columns (Cytiva) for Ni²⁺ affinity chromatography. The column was then equilibrated in wash buffer (20 mM Tris, 300 mM NaCl, 10 mM imidazole, pH 8), before the protein was eluted with elution buffer (20 mM Tris, 300 mM NaCl, 500 mM imidazole, pH 8), in a ratio of 1:3 to wash buffer. The protein was further purified using a 5ml HiTrap DEAE Sepharose FF Ion Exchange chromatography column (Cytiva) for ion exchange purification. A gradient elution of 0-100% elution buffer (25 mM Sodium phosphate pH 7.4, 0-500 mM NaCl) was performed over 300 ml. The protein was then purified by size exclusion chromatography (HiLoad 26/600 Superdex 75 pg, Cytiva) and eluted in 25 mM Sodium Phosphate, pH 7.4. The purified protein was dialysed into MilliQ water and freeze-dried for storage at -20°C.

Hydrogel Preparation

$I27_5$ was re-suspended in 25 mM sodium phosphate, pH = 7.4 and placed on a rotary wheel for a minimum of 1 h to enable complete dissolution of protein. The suspensions were then centrifuged for 10 minutes at 5000 RCF, retaining the supernatant to ensure that any insoluble protein was removed. Protein concentration was measured by absorption at 280 nm, using an extinction coefficient of $43824\text{M}^{-1}\text{cm}^{-1}$. The final suspension was then diluted and mixed with an assembly buffer of Tris(2,2'-bipyridyl)-dichlororuthenium(II) hexahydrate (Ru(BiPy)₃) and sodium persulfate (NaPS) directly before use, with final concentrations of 0.38 mM $I27_5$, 100 μM Ru(BiPy)₃ and 10 mM NaPS. Sample gelation was initiated photochemically through 60 seconds of in-situ illumination with a 460 nm light emitting diode as previously described [31]. The illumination intensity was calibrated to $40\text{ mW}\cdot\text{cm}^{-2}$ at 452 nm.

Shear Rheology

Rheology measurements were performed using a stress-controlled rheometer (Kinexus Malvern Pro) equipped with a 10 mm steel plate and plate geometry. The lower plate of the rheometer was replaced with a custom-built photodiode module which allowed the photochemical crosslinking to be carried out in-situ. To prevent the evaporation, low viscosity (5 cSt) mineral oil was applied to the air-sample interface. All measurements were performed at 25 °C and 2 hours after crosslinking. For all measurements, rheology data was captured over at least 3 measurements on independently prepared samples.

Small Amplitude Oscillatory Measurements

All small amplitude oscillatory measurements were carried out at a strain amplitude of 1% - comfortably within the linear viscoelastic regime for all samples studied. Time dependent measurements were carried out at an angular frequency of 6.28 s^{-1} unless otherwise stated. At high frequencies, artifacts from instrument inertia were avoided by discounting all data points for which the phase angle exceeded 150°.

Cyclic Loading Measurements

Cyclic loading experiments were performed to probe the mechanical response of the polyprotein hydrogel to large deformations and to examine the effect of multiple deformations on the hydrogel mechanics. Following crosslinking, the sample was subjected to a shear strain pulse of loading rate 0.01 s^{-1} . After each pulse, the sample was left to recover for 23 min, during which time a single oscillatory frequency sweep was carried out to assess any permanent changes to material properties. The process was then repeated with incrementally increasing strain pulse magnitudes.

Stress relaxation

Stress relaxation experiments were carried out by applying a step strain to the sample for 10 mins. The resulting relaxation in stress over time was fitted to a range of different constitutive models using the Rheology Open Source (RHEOS) software. [32,33] A constant applied strain was typically attained within 2-3 s and any data from before this point were discarded from the analysis.

Circular Dichroism

Circular dichroism (CD) measurements were performed on an Applied Photophysics Chirascan CD spectropolarimeter using 0.01 mm path length cuvettes at a concentration of 0.5 mM. Samples were gelled inside the cuvette through photochemical crosslinking using identical buffers and the same protocol to that used in shear rheology experiments. Samples were also probed at higher dilution ($5 \mu\text{M}$), in which case the protein was probed in a phosphate buffer without crosslinking agents (25 mM sodium phosphate, $\text{pH} = 7.4$) in a 1mm path length cuvette. Each measurement was averaged over 1 s and any data points for which the photomultiplier tube voltage (HV) exceeded 600 V were not included in the analysis. A minimum of 4 independently prepared samples were used for each measurement to ensure reproducibility. Standard deviations did not exceed 10% of the mean value.

Results

I27 Protein Structure is Retained following Crosslinking

The $I27_5$ polyprotein comprises five sequential repeats of the $I27$ as shown in figure 1 (a). The $I27$ polyproteins are assembled into hydrogels using the well-known ruthenium crosslinking strategy, [34] which causes tyrosine residues on the surface of the polyproteins to radicalise and form dityrosine linkages under illumination of visible light and in the presence of sodium persulfate. Each polyprotein has five native tyrosine sites which are retained in the polyprotein design. The polyprotein also contains a hexahistidine repeat at its N-terminus and a dicysteine residue at its C-terminus, both of which are known to crosslink under the same conditions, albeit at lower efficiency. [35] Therefore the polyprotein can be said to possess 7 potential crosslinking sites. The sodium persulfate that drives the crosslinking reaction is present at an approximately $4\times$ stoichiometric excess to the potential crosslink sites therefore we may assume a high crosslinking efficiency. Recent computational work from our group has predicted that the coordination efficiency of pentameric polyproteins with a similar number of crosslinks to $I27_5$ is close to unity, [21] therefore without making a priori assumptions about the meso-scale structure, it can already be assumed that the network is densely crosslinked, with each polyprotein being permanently crosslinked to multiple neighbouring polyprotein molecules.

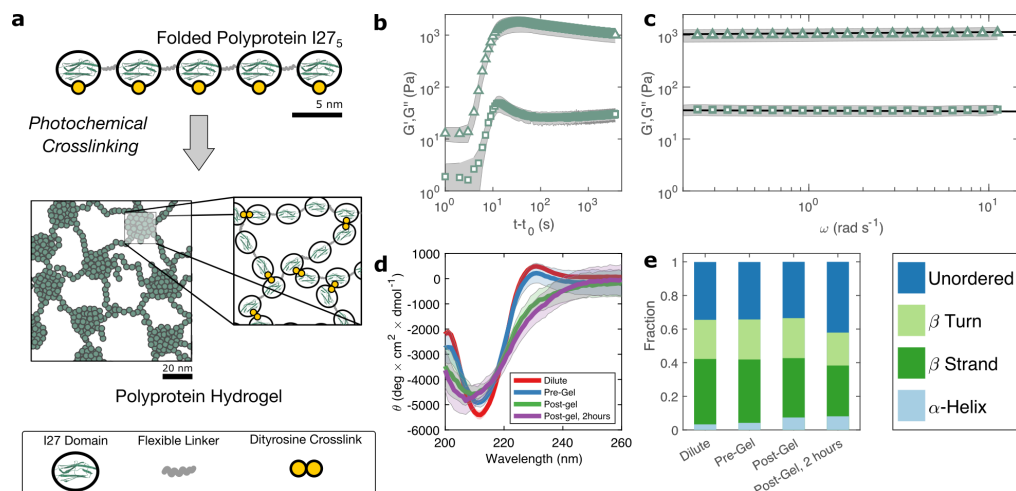


Figure 1. (a) The polyprotein used in this study comprises five concatenated I27 domains inter-spaced with flexible 'linker' regions. Illumination of polyprotein solutions with 490 nm blue light in the presence of crosslinking reagents leads to gelation through the formation of dityrosine bonds. (b) A sharp increase in G' (triangles) and G'' (squares) over a timescale of seconds indicates rapid crosslinking. (c) Within the linear viscoelastic regime, after 2 hours both G' and G'' exhibit a weak power law dependence on frequency (d) Circular dichroism spectra show a β -sheet peak at 211 nm, with a slight peak shift and decrease in intensity after gelation. (e) Analytical fitting spectra using the CONTINLL reference set confirms the structure is predominantly β -sheet, before and after gelation and indicates reduction in the fraction of folded protein of approximately 12%, taking place at equivalent timescales to the decrease in G'/G'' . Error bars in (b)-(d) (shaded regions) represent averaged measurements.

To probe this crosslinking process, we carry out small amplitude oscillatory shear measurements, probing the storage (G') and loss (G'') moduli of the sample during *in situ* illumination at time $t = t_0$. As plotted in figure 1(b) there exists a short lag time before a sharp increase is observed in both G' and G'' . In a recent study of globular bovine serum albumin (BSA) hydrogels we showed that this lag time [31] is strongly indicative of a two-step nucleation and growth process, in which diffusion-limited pre-gel clusters mature towards eventual percolation. Although the intensity of light and the stoichiometric ratio are similar to this previous study, the observed lag time is significantly shorter (~ 3 s) for $I27_5$ than for BSA (~ 30 s).

The value of G' and G'' both increase sharply following the lag phase, reaching a peak of $1.7 \pm 0.6 \times 10^3$ Pa after approximately 30 s, before undergoing a steady decrease and reaching a final G' of $1.0 \pm 0.3 \times 10^3$ Pa, after approximately 1 hr. To examine the possible molecular origins of this decrease in moduli, we carry out CD spectroscopy across each stage of the crosslinking process as shown in figure 1(d). Before crosslinking the mean residue ellipticity spectrum indicates an anti-parallel β -sheet structure which, in $I27$, is typically characterised by a negative band at 211 nm [36]. A slight positive band can also be seen close to 230 nm, which reflects exciton coupling between aromatic residues [37, 38]. Compared with the spectra of dilute uncrosslinked $I27_5$, there is a close alignment ($< 10\%$ difference in peak at 211 nm) indicating that the protein remains largely stable at the increased concentrations used for gelation, while the magnitude of the 211 nm band ($5.4 \pm 0.2 \times 10^3$ deg. cm². dmol⁻¹) is comparable to previous studies of $I27_5$. Following photochemical crosslinking, the peak intensity reduces and shifts to a lower wavelength, which may indicate a decrease in the folded protein fraction. Assuming that the 211 nm peak intensity is directly proportional to

	β - Strands	β - Turns	Unordered
Dilute (5 μ M)	0.39	0.23	0.34
Pre- Crosslink	0.38	0.24	0.34
Post- Crosslink	0.35	0.24	0.34
Post-Gel, 2 hrs	0.30	0.20	0.42

Table 1. Secondary structure composition of I27₅ polyprotein hydrogels. α -helix content (not shown) is the result of deconvolution errors.

the fraction of folded protein, we estimate a reduction in folded fraction of I27₅ of 7%. The 230 nm peak is also reduced, presumably due to the conversion of the aromatic tyrosine residues into dityrosine residues during crosslinking. Overall, this indicates a slight reduction in the folded fraction of I27₅. To investigate this further, we deconvoluted the CD spectra using the CONTINLL parameter set in Dichroweb [39], using protein reference set 4 (optimised for 190 - 240 nm). As shown in figure 1(e), table 1, and figure S3 there is a slight reduction in β -sheet fraction and β -turn fraction and an increase in the proportion of the protein that is unordered. Taking this as being indicative of protein unfolding under gelation, we estimate a decrease in the fraction of folded protein of approximately 12%, which takes place in the 2 hours following gelation, the same time over which a decrease in G' and G'' is observed. A similar reduction in folded fraction that coincides with a decrease in G' and G'' has previously been observed for other folded protein hydrogels studied in our group [22, 23, 31], which suggests that it is a general feature of folded protein hydrogels, where it is caused by forced unfolding of weak protein domains on the *molecular*-scale as the hydrogel network forms.

Frequency Sweeps Indicate a Fractal Network Structure

Rheological frequency sweeps (figure 1(c)) show that the equilibrated hydrogels are predominantly elastic in nature, with a storage modulus G' that is over an order of magnitude higher than the loss modulus G'' across all probed frequencies. Frequency sweeps reflect the distribution in timescales of the underlying relaxation mechanisms in the hydrogel. For our I27₅ hydrogels we find that the frequency dependence of G' and G'' are well-described by weak power law relationships (solid lines in figure 1(c)). The physical origins of this power law viscoelasticity in hydrogels remain a matter of debate [40] but they are commonly associated with fractal structure in a variety of soft and biological materials [24, 40–49]. In recent work from our group, we have shown that fractal structures are also present in folded protein hydrogels [22, 23] and that these structures arise from the diffusion- and rate-limited crosslinking of constituent folded proteins [31] and *in situ* protein unfolding. [22, 23]

The emergence of a power law relaxation spectrum can be rationalised by considering that a fractal hydrogel network has a self-similar structure and consequentially will exhibit self-similar relaxation dynamics. [44] Assuming that the excluded volume interactions are screened, this allows the fractal dimension d_f of the hydrogel network to be directly calculated using the following previously derived [24] relation:

$$\beta = \frac{3(5 - 2d_f)}{2(5 - d_f)} \quad (1)$$

where $G' \sim \omega^\beta$ and $0 < \beta < 1$, which correspond to $1.25 < d_f < 2.5$. The above

relation was originally devised for gels at the percolation threshold but has also been shown to be broadly applicable at later timescales, [40] as used here. A simple least squares fit to figure 1(c) reveals a weak power law ($\beta = 0.02$). We also independently verify the value of β using the Kramers-Kronig relation: $G''/G' = \tan(\beta \times \pi/2)$ which is a consequence of the interdependence between G'' and G' . [50] We find $\beta = 0.022 \pm 0.002$ (figure S2, supplementary), in excellent agreement with the power law fit. Taking $\beta = 0.02$, equation (1) indicates a fractal dimension of 2.48. In previous work we have carried out structural characterisation of *I27₅* hydrogels [29], which revealed dense nanoscale clusters of polyproteins with a mean diameter of 20 nm, surrounded by sparser inter-cluster regions, which may be either folded [23] or unfolded [22], depending on the constituent protein. These nanoscale clusters have been shown to be fractal in nature with values of d_f across a broad range 2.1-2.7. [23] How then should we compare the value of d_f of the nanoscale clusters to those extracted from time-dependent rheology data? The rheological response of folded protein hydrogels is likely [31] to depend not on the structure of the nanoscale clusters but rather on the connectivity of inter-cluster regions. This is analogous to colloidal gels, in which the hydrogel elasticity is a property that emerges from the density of connections *between* colloidal clusters. [51] Our analysis is therefore reminiscent of other soft matter systems and intriguingly points towards the possibility of a fractal structure that is *length-scale dependent*. Although we cannot infer the precise length scale of the inter-cluster regions through rheology, recent work from our group has measured this length scale for MBP hydrogels as being approximately 100 nm. [23]

Hydrogel Structure is Responsive to Deformation

So far, we have identified that the relaxation spectrum of an *I27₅* hydrogels can be functionally fitted to a power law model, with exponent β . To validate this, we independently carry out a series of stress relaxation experiments, in which a step strain is applied to the sample and the sample's shear stress decays over time. This approach avoids the changes in sample strain that are inherent to creep measurements while also probing a longer range of timescales than oscillatory frequency sweeps. We probe the extent of the linear viscoelastic regime through a shear strain ramp (figure S4), which confirms that the linear viscoelastic regime corresponds to $\gamma < 0.1$, with only a slightly nonlinear response at higher strains ($\gamma < 0.3$). While the exponent β is easily extracted from the frequency sweeps, extracting it from relaxation data requires a mechanical constitutive modelling approach. Here, elements of Hookean elasticity (springs) and Newtonian viscosity (dashpots) are combined in an empirical manner to approximate the viscoelastic response. In many materials, a finite number of such elements are sufficient, [52] however for power law viscoelasticity the spectrum of relaxation times is broad and hence the approach requires a large number of fitting parameters making it unsuitable. [53] To address this, we use a so-called fractional rheological model, which captures power law rheology using a minimal number of fitting parameters. This is achieved by reducing an arbitrary large number of springs and dashpots (figure 2 (a)) to a single mathematical element commonly known as a springpot model [54] with two fitting parameters β and c_β . The parameter c_β , is often referred to as a *quasi-property* [53] since its SI units ($\text{Pa}\cdot\text{s}^\beta$) contain a power law exponent. From a practical perspective c_β can most simply be conceptualised as referring to the 'firmness' or 'strength' of the material [55]. The springpot model describes stress relaxation $\sigma(t)$ following an applied step strain γ over a measurement timescale t as:

$$\sigma(t) = c_\beta \frac{d^\beta \gamma}{dt^\beta} \quad (2)$$

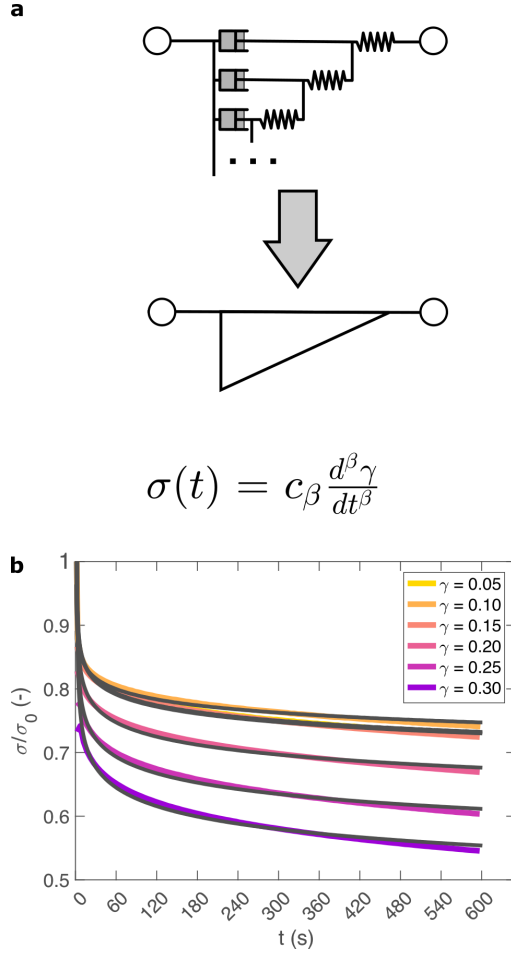


Figure 2. (a) Relaxation data are fitted using a fractional model, which represents an arbitrarily large network of springs and dashpots, using just two parameters c_β and β . (b) A step strain γ at time 0 is applied to an $I27_5$ hydrogel and the normalised stress response σ/σ_0 is probed. The model (grey line) provides an excellent fit across a range of values of γ .

Here β has the same physical meaning as previously defined. The elegance of the above relation is reflected in the fact that it reduces to the equation for a Hookean spring when $\beta = 0$ and to a Newtonian dashpot when $\beta = 1$. The underlying physical basis for this model is supported by the fact that when fractal soft materials are embedded with passive particles, the particle motion is sub-diffusive and anomalous ($\langle \Delta x^2 \rangle \sim t^\beta, \beta < 1$). [56, 57] This sub-diffusive behaviour arises from the multi-scale structure of the material which also directly leads to power law stress relaxation. [58] As such, the fractional approach has come to be established as the most predictive model for power-law viscoelastic materials. [40, 54, 59, 60]

As shown in figure 2(b), equation 2 provides an excellent fit to the stress relaxation data, both within the linear viscoelastic regime ($\gamma < 0.1$) and even for the nonlinear regime ($0.1 < \gamma < 0.3$). For step strains that exceed this strain (figure S5) we consistently observe an instantaneous decrease in stress during the measurement, suggesting that the sample undergoes irreversible fracture. The fitted parameters β and c_β are shown in figure 3.

The fractional model provides an excellent fit to the relaxation data. We also

attempted to fit several different variations of the two-component fractional model, incorporating different combinations of springs, dashpots and springpots arranged in series and in parallel in attempt to improve our model. The use of either fractional Maxwell model (two springpots in series, figures S6 [61]) or a modified power law model (springpot combined with a dashpot and spring, figure S7 [33]) provide a poor fit to the data as both predict a plateau in $\sigma(t)$ at long timescales. A fractional Kelvin Voigt model (two springpots in parallel, figure S8) does provide a close fit to the data, however the additional parameters are degenerate to fitting.

Within the linear viscoelastic regime, the value of β is independent of applied strain, as expected, and has an average measured value of 0.03 ± 0.01 . This is in excellent agreement with the frequency spectra ($\beta = 0.02$), demonstrating that the power-law model accurately predicts the viscoelastic material properties of the $I27_5$ hydrogels, which are likely to originate from a cross length-scale fractal structure. Interestingly, the springpot model appears to provide an excellent fit to the relaxation data at strains that exceed the linear viscoelastic regime. The reasons for this are not immediately clear since the fractional model that we employ is only strictly valid for linear viscoelastic materials, [62] although attempts have been made to extend it to nonlinear behaviour. [47, 63] It may be that the deviations from linear viscoelasticity for $0.1 < \gamma < 0.3$ (figure S4) are sufficiently minor so as not to invalidate the model. We find that c_β increases with strain, which suggests a strengthening of the hydrogel network. This, accompanied by an increase in β over the same range of applied strain, suggests progressive changes in network structure as the strain is increased. β reaches a maximum of 0.065 ± 10^{-5} for γ , which using the equation (1), would correspond to a slight decrease in fractal dimension from $d_f = 2.47$ to $d_f = 2.44$. Assuming that our model is indeed valid at higher strains, we propose that this change may reflect the progressive unfolding of the constituent $I27$ domains as the applied strain is increased, leading to changes in the hydrogel network structure. At the same time, the increase in c_β would imply a strengthening or reinforcement of the network at increased strain. One explanation for this is that the polyprotein chains stiffen, by aligning with the direction of shear (leading to an increase in c_β) while simultaneously unfolding (leading to an increase in β).

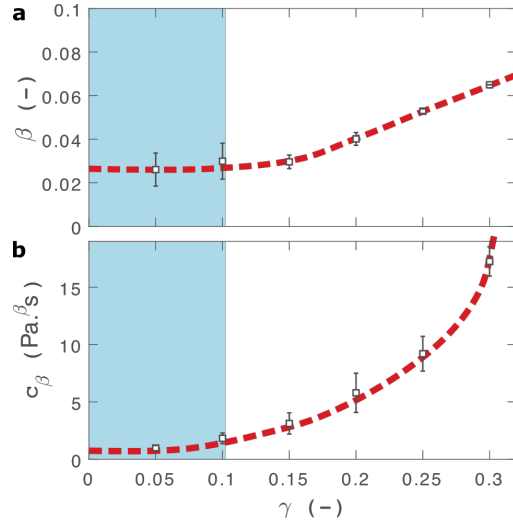


Figure 3. Fractional fit parameters extracted from applying equation 2 to data in shown in figure 2. The shaded region indicates the linear viscoelastic regime. Dashed lines are guides for the eye. Error bars represent fits over multiple measurements

Comparison can be made to a previous study by our group on crosslinked BSA

hydrogels. In that study, the addition of a reducing agent resulted in breakage of covalent bonds within the BSA protein, resulting in a more force labile protein. [22] Upon cross-linking, *in situ* protein unfolding was found to define the network architecture and mechanics, with regions of clusters of folded protein interconnected by unfolded protein. The study also noted an increase in the power law exponent when the disulphide bonds that prevent unfolding of the protein were broken through chemical reduction. Remarkably, the power law exponents before and after covalent bond breaking (0.027 ± 0.002 and 0.061 ± 0.001 , respectively) are almost identical to the exponents at low and high strains measured here (0.03 ± 0.01 and 0.065 ± 10^{-5} , respectively), providing further support for our hypothesis that the structural changes implied by our data arise from the force induced unfolding of individual protein domains.

Nonlinear Mechanics Indicate Reversible Alignment and Unfolding of Polyproteins

How do the structural properties of $I27_5$ hydrogels that we have encountered, change under deformation? Our relaxation data show intriguing clues that suggest network strengthening and unfolding under applied strain. To probe this independently we carry out nonlinear cyclic deformation experiments [64,65]. As depicted in figure 4(a) and figure S9, the $I27_5$ polyprotein network is loaded and unloaded up to a threshold strain γ_{max} through a triangular strain pulse at a constant shear rate and the magnitude of γ_{max} is increased with each subsequent shear pulse.

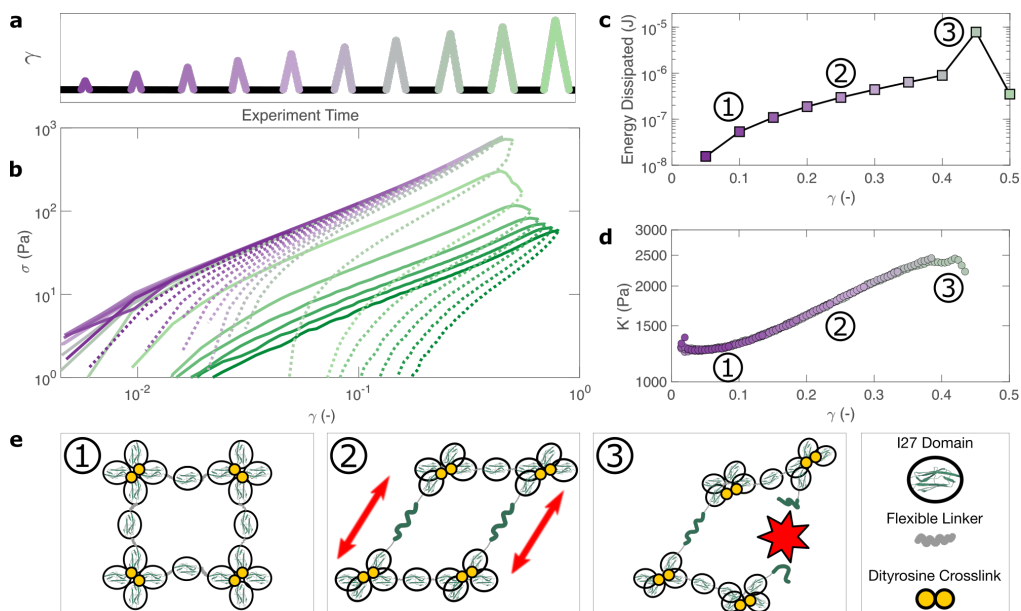


Figure 4. The bulk response of polyprotein networks under large deformation reveals insights into the mechanisms of energy dissipation. A series of triangular strain (γ) pulses of increasing magnitude are applied (a). For $\gamma < 0.4$ each stress (σ) curve overlays closely with its predecessor (b) indicating that the hydrogel’s mechanical response is fully reversible. Increasing applied strain correlates closely with energy dissipation (c) and strain stiffening (d), which are macroscopic manifestations of the unfolding of individual protein domains and the stretching of polyproteins, respectively. This is shown diagrammatically (e). At $\gamma = 0.4$ the energy dissipated increases sharply and subsequent loading curves no longer overlay, indicating the irreversible fracture of the hydrogel.

Within the linear viscoelastic regime, ($\gamma_{max} < 0.1$) the loading and unloading curves (figure 4 (a), solid and dashed lines respectively) appear to overlay closely suggesting a reversible and purely elastic response. However as γ_{max} increases, a deviation between the loading and unloading curves begins to emerge. Calculating the energy loss in each cycle (4(c)) from the ratio of the areas beneath the loading and unloading curves (see methods), shows that inelastic energy dissipated during loading steadily increases with γ_{max} . Furthermore, each subsequent loading curve appears to overlay with its predecessor, indicating that this inelastic dissipation does not bring about any permanent changes to the network stiffness. This complete reversibility of the network is unusual as most polymer networks that exhibit reversibility, such as filled rubbers [66] and biological tissues also exhibit a well-defined residual cyclic softening. By contrast, we observe an almost perfect overlay between loading curves for strains up to $\gamma = 0.4$. The profile of the loading curves is also revealing of changes in hydrogel stiffness during deformation. For $\gamma > 0.1$, the stress σ required to increase the strain becomes progressively higher, indicating strain-stiffening. [67] This can be most clearly seen in the evolution of the differential elastic modulus K' with respect to strain (figure 4(d)), which increases approximately by a factor of 2 before the onset of rupture. As with the loading curves, the relationship between K' and γ overlays closely across all curves, confirming that no softening takes place between loading cycles. Plotting K' with respect to σ , reveals that the stiffening follows a power law relationship of $K' \sim \sigma^{0.6}$ (figure S10). Such power law stiffening is a general feature of semiflexible networks for which the distance between crosslink nodes is similar to the polymer persistence length and arises from the entropic resistance of thermal undulations against stretching. [67] To assess whether our system can be considered to be semiflexible we carry out an analysis of the polyprotein dimensions (see supplementary information) which reveals that the distance between the crosslink sites is 5.44 nm. To calculate the persistence length of the polyproteins we draw on our previous computational calculations for a range of polyprotein dimensions. [19] The most important parameter here is the ratio between the length of the linker domain and the radius of the globular domains, which for our dimensional analysis is ≈ 0.34 . This corresponds [19] to a persistence length in the range of ≈ 7 -14 nm. Therefore, the persistence length and crosslink length are of the same order of magnitude and the polyprotein can be considered as semiflexible. For semiflexible networks it is expected that $K' \sim \sigma^{1.5}$ [68] although exponents as low as 0.5 [69] have been observed elsewhere and are thought to arise from inelastic effects such as crosslink unbinding or axial stretch.

For our system, strain stiffening appears to occur concurrently with energy dissipation, which agrees with the stiffening and dissipation hypothesis that emerges from our relaxation data. From the strain ramp data, it seems likely that strain stiffening occurs due to the stretching of the constituent semiflexible polyproteins and that these polyproteins undergo force-induced unfolding concurrently (figure 4 (e)).

Fracture of Polyprotein Hydrogels is Driven by Structural Adaption

If the unfolding and refolding of $I27_5$ in the hydrogel is indeed reversible then how does the fracture, as observed from strains exceeding 0.4, take place? To investigate this further, we carry out oscillatory frequency sweep measurements after each of the triangular strain pulse measurements. Each frequency sweep therefore represents the linear viscoelastic properties of the hydrogel after each cycle of deformation. The profiles of the individual frequency sweeps of the hydrogels remain highly reproducible at pre-fracture strains, (figure S12) which is consistent with our previous observation that the deformations are fully reversible. At higher strains, the linear elastic modulus G' begins to decrease (figure 5 (a)). Over the same strain range, the power law exponent of the frequency sweeps β increases, (figure 5 (b)) indicating permanent

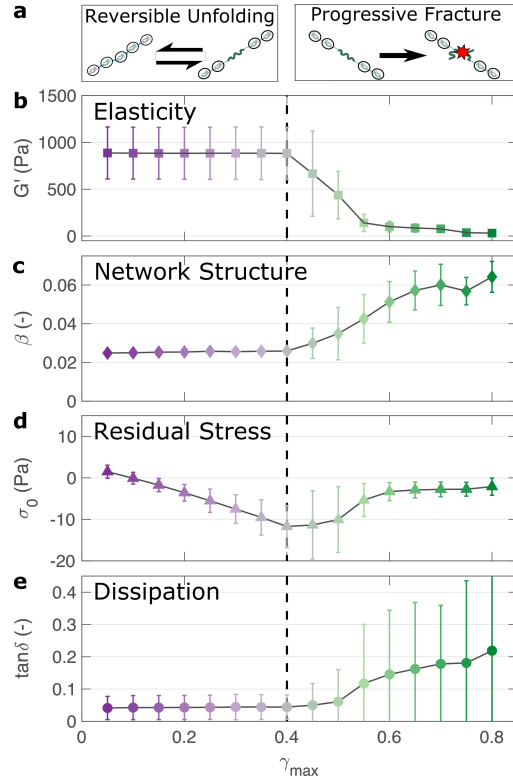


Figure 5. The linear viscoelastic properties of the *I27*₅ hydrogels after strain pulse deformation cycles of magnitude γ_{max} reveal the fracture properties of the hydrogel network (a). The elastic modulus remains unchanged below a threshold strain of $\gamma_{max} = 0.4$, after which it steadily decreases, indicating network fracture (b). The power law exponent β , which represents the fractal structure of the hydrogel increases after the fracture point, indicating structural changes post-fracture (c). The negative stress σ_0 needed to return the network to zero strain after each deformation cycle steadily increases before fracture, suggesting a build-up of tension after each deformation cycle (d). Meanwhile the network dissipation ($\tan\delta = G''/G'$) remains relatively low over all values of γ_{max} , indicating that bond rupture rather than protein unfolding is the underlying cause of the fracture of the hydrogel network above a threshold strain of $\gamma_{max}=0.4$.

structural change, even after the removal of strain. At this final stage, the value β reaches 0.064 ± 0.008 . Remarkably, this is identical to the maximum value of β measured through stress relaxation experiments (Figure 3).

The fracture of biopolymer networks is a complex phenomenon that is challenging to model. [70] In network-forming systems, fracture typically occurs suddenly and is preceded by a dynamic microscopic changes [71]. The eventual mechanism of fracture can originate from the dissociation of noncovalent bonds, the permanent rupture of covalent bonds, or both concurrently. [72] We expect that covalent bond rupture is the most likely cause in our system since the hydrogels are covalently crosslinked. Furthermore, the high energy dissipation at $\gamma_{max} < 0.4$ (figure 4) implies protein unfolding occurs pre-rupture. This observation is consistent with the unfolding forces of an *I27* domain (~ 0.2 nN [27]), which are lower than the typical rupture forces of a covalent bond ($\sim 1-2$ nN [73] at a pulling speed of 10 nN.s⁻¹). One possible mechanism for fracture is that as the polyprotein approaches a fully unfolded state, the tension that

was previously directed to domain unfolding instead is applied to the unfolded polypeptide chain leading ultimately to irreversible peptide bond rupture. It is intuitive that such rupture would occur at the weakest bond in the chain, in this case a peptide bond in either the unfolded *I27* domains or the linker region. Further evidence for the mechanism of rupture can be found by re-examining the strain pulse data in figure 4. Specifically, the stress required to return the hydrogel to zero strain after each pulse is denoted σ_0 (shown diagrammatically in figure S11). This represents the residual stress after each deformation cycle. σ_0 is initially close to 0 and becomes more negative after each cycle until the onset of fracture (figure 5(c)). Post fracture, σ_0 no longer becomes more negative, which may reflect the loss of tension in the network as the polyprotein chains rupture. Finally, the value of $\tan\delta$ (figure 5 (d)), which quantifies the relative viscous dissipation of the network in the form of the ratio between the elastic and viscous moduli, remains relatively low (≈ 0.2 , at the highest values of γ_{max}). Given that the chains are highly dissipative at high strains (figure 4 (d)) and given the theoretical range of $\tan\delta$ (0-1), a much higher dissipation would be expected if the polyprotein chains remained intact but unfolded. It is therefore likely that the network fracture is determined by the reversible unfolding of the protein domains which, at significantly high tension leads to eventual bond rupture as shown diagrammatically in figure 5 (e).

Discussion

In summary, we have applied a multi-modal rheology approach to interrogate the viscoelastic properties of folded protein hydrogels. Using these approaches, we highlight several important and previously unappreciated aspects of their material properties.

Firstly, we determine that the viscoelasticity of *I27*₅ hydrogels can be accurately modelled by a simple two-parameter fractional viscoelastic constitutive model. This model manifests itself as a power law in both the frequency response (figures 1 (c) and S12) and in the time-dependent stress relaxation response (figure 2). From a practical perspective, this indicates that hydrogel's stress relaxation is governed not by a single characteristic timescale but rather by a broad spectrum of timescales. This is perhaps surprising as it suggests that the viscoelastic response of the hydrogel, at least within the linear viscoelastic regime, is not governed primarily by the narrow and well-defined unfolding timescale of the *I27* protein domains when stretched axially. [15] Instead the architecture of the hydrogel appears to result in a more complex spectrum of relaxation timescales, which likely arises from the orientation and arrangements of the protein domains. There are several possible mechanisms to explain this behaviour. Firstly, it could be argued that the formation of the hydrogel network causes partial unfolding, however we show a reduction of the fraction of folded protein of just 12% (figure 1). A more likely explanation is that the fractal structure of the hydrogel [22, 23, 31] leads to a broad spectrum of relaxation modes, which reflects the broad spectrum of length scales within the network. [74] One additional contributing factor could be the random alignment of the polyprotein chains within the hydrogel network in relation to the direction of shear deformation. In principle this could lead to changes in the relaxation timescales as the mechanical stiffness of folded proteins is known to depend on their pulling geometry [75]. The broad spectrum of relaxation times we observe here appears to be common in polymeric systems [76], cells [33, 77] and tissues [78]. Here, we show that this behaviour also extends to folded protein hydrogels.

Using a fractional viscoelastic model, we show that the power law exponent β is remarkably consistent between the oscillatory shear and stress relaxation experiments used in this study. Therefore, we may say that power law viscoelasticity is not an artifact of any particular technique but is instead an intrinsic property of the hydrogel and is likely to reflect the hydrogel's fractal structure. A consistent value of β is also measured after multiple cycles of deformation, indicating that this fractal structure is

robust to perturbation. More surprisingly, our model also closely fits the relaxation response at larger deformations in the nonlinear viscoelastic regime (figure 3(a)). While our model is strictly valid only for linear viscoelasticity, we note that the fitted parameter β in this regime is close to the value of β as probed by oscillatory shear after the hydrogel fracture. We speculate that this may be indicative of permanent changes to the hydrogel’s structure at large deformations. Modelling this behaviour using more advanced constitutive modelling that accounts directly for nonlinear effects [47, 63] would be an interesting topic of further study.

Within this nonlinear regime we observe that the hydrogel undergoes stiffening while subjected to shear strains, which is manifested both in relaxation data (figure 3 (b)) and in strain ramp data (figure 4 (d)). In line with predictions, [19] this is consistent with the semiflexible nature of the polyprotein chain, a property that arises directly from the dimensions of the folded proteins. Recreating strain stiffening in synthetic hydrogels is a growing area of research [79] and although the degree of stiffening is relatively low for this system (a twofold increase in modulus before fracture) it is likely that a modification of the polyprotein dimensions could tune and enhance this behaviour further.

This strain-induced stiffening occurs at low strains, which corresponds to the onset of nonlinearity in stress relaxation experiments (figure 2) and to an observed increase in energy dissipation (figure 4 (d)). Our relaxation data indicates an increase in the power law exponent β during deformation but notably there is no permanent changes to the hydrogel’s viscoelasticity or β (figure 5), suggesting that the network structure is not significantly altered by repeated deformation. This stands in direct contrast to conventional rubber materials, in which the viscoelastic response from each subsequent deformation cycle is directly determined by the strain history of the sample. [66] It is likely that this behaviour is a consequence of the *I27* domain’s propensity to re-fold upon removal of stress, since the same behaviour has been observed for hydrogels constructed from the similarly reversible GB1 domains. [9] Nevertheless, our analysis of the repeated loading curves indicates that some stress accumulates in the network after each deformation cycle (figure 5(d)), which likely contributes to its eventual fracture.

Finally, we wish to re-emphasise that the weak power-law rheology that we observe here is also commonly observed in biological tissue. Indeed, slow internal relaxation processes appear to be intrinsic to a broad range of living materials [63]. The mechanical similarities between biological tissues and folded protein hydrogels are apparent and may provide further support for their potential applications in replacing and repairing living tissue.

In summary, we have shown that the viscoelastic response of *I27*₅ folded protein hydrogels is governed not only by the molecular mechanics of the folded protein domains, as has commonly been assumed, but also by their meso-scale structure. Within the linear viscoelastic regime, the protein domains remain folded, and the response follows a characteristic power-law rheological behaviour. This is well described by a fractional viscoelastic model and most likely arises from the hydrogel’s fractal structure. At higher strains, nonlinear viscoelasticity is observed in the form of strain stiffening, which is accompanied by an increase in energy dissipation as the polyprotein chains align and unfold. This unfolding shows an excellent degree of reversibility, which affirms the ability of the constituent *I27* domains to return to their folded conformation upon removal of stress. Overall, we show that folded protein hydrogels exhibit a rich diversity of viscoelastic properties which reflect the hierarchy of length-scales, from their energy-dissipative properties (at the length scale of individual proteins) to their stiffening (at the length scale of polyprotein chains) and their linear viscoelasticity and fracture properties (at the length scale of the hydrogel network). We expect that these insights will be instructive in the continuing efforts to modify and control the mechanics

of folded protein hydrogels as well as for their envisaged applications as biomaterials.

References

1. Enrica Caló and Vitaliy V. Khutoryanskiy. Biomedical applications of hydrogels: A review of patents and commercial products. *European Polymer Journal*, 65:252–267, April 2015.
2. Armin Vedadghavami, Farnaz Minooei, Mohammad Hossein Mohammadi, Sultan Khetani, Ahmad Rezaei Kolahchi, Shohreh Mashayekhan, and Amir Sanati-Nezhad. Manufacturing of hydrogel biomaterials with controlled mechanical properties for tissue engineering applications. *Acta biomaterialia*, 62:42–63, 2017.
3. Robert Langer and David A Tirrell. Designing materials for biology and medicine. *Nature*, 428(6982):487–492, 2004.
4. Federica Burla, Yuval Mulla, Bart E Vos, Anders Aufderhorst-Roberts, and Gijse H Koenderink. From mechanical resilience to active material properties in biopolymer networks. *Nature Reviews Physics*, 1(4):249–263, 2019.
5. Matt D. G. Hughes, Sophie Cussons, Najet Mahmoudi, David J. Brockwell, and Lorna Dougan. Tuning protein hydrogel mechanics through modulation of nanoscale unfolding and entanglement in postgelation relaxation. *ACS Nano*, 2022.
6. Shanshan Lv, Yi Cao, and Hongbin Li. Tandem modular protein-based hydrogels constructed using a novel two-component approach. *Langmuir*, 28(4):2269–2274, 2012.
7. Luai R Khoury and Ionel Popa. Chemical unfolding of protein domains induces shape change in programmed protein hydrogels. *Nature communications*, 10(1):1–9, 2019.
8. Junhua Wu, Pengfei Li, Chenling Dong, Heting Jiang, Bin Xue, Xiang Gao, Meng Qin, Wei Wang, Bin Chen, and Yi Cao. Rationally designed synthetic protein hydrogels with predictable mechanical properties. *Nature communications*, 9(1):1–11, 2018.
9. Shanshan Lv, Daniel M. Dudek, Yi Cao, M. M. Balamurali, John Gosline, and Hongbin Li. Designed biomaterials to mimic the mechanical properties of muscles. *Nature*, 465(7294):69–73, May 2010.
10. Na Kong, Linglan Fu, Qing Peng, and Hongbin Li. Metal chelation dynamically regulates the mechanical properties of engineered protein hydrogels. *ACS Biomaterials Science & Engineering*, 3(5):742–749, 2016.
11. Linglan Fu, Amanda Haage, Na Kong, Guy Tanentzapf, and Hongbin Li. Dynamic protein hydrogels with reversibly tunable stiffness regulate human lung fibroblast spreading reversibly. *Chemical Communications*, 55(36):5235–5238, 2019.
12. Luai R Khoury, Marina Slawinski, Daniel R Collison, and Ionel Popa. Cation-induced shape programming and morphing in protein-based hydrogels. *Science advances*, 6(18):eaba6112, 2020.

-
13. Qingyuan Bian, Linglan Fu, and Hongbin Li. Engineering shape memory and morphing protein hydrogels based on protein unfolding and folding. *Nature communications*, 13(1):1–8, 2022.
 14. Rafayel Petrosyan, Abhishek Narayan, and Michael T Woodside. Single-molecule force spectroscopy of protein folding. *Journal of Molecular Biology*, 433(20):167207, 2021.
 15. M. Rief. Reversible unfolding of individual titin immunoglobulin domains by AFM. *Science*, 276(5315):1109–1112, May 1997.
 16. Toni Hoffmann, Katarzyna M Tych, Megan L Hughes, David J Brockwell, and Lorna Dougan. Towards design principles for determining the mechanical stability of proteins. *Physical Chemistry Chemical Physics*, 15(38):15767–15780, 2013.
 17. Chase P Broedersz and Fred C MacKintosh. Modeling semiflexible polymer networks. *Reviews of Modern Physics*, 86(3):995, 2014.
 18. Kirill Shmilovich and Ionel Popa. Modeling protein-based hydrogels under force. *Physical review letters*, 121(16):168101, 2018.
 19. Benjamin S. Hanson, David Head, and Lorna Dougan. The hierarchical emergence of worm-like chain behaviour from globular domain polymer chains. *Soft Matter*, 15(43):8778–8789, 2019.
 20. Benjamin S Hanson and Lorna Dougan. Network growth and structural characteristics of globular protein hydrogels. *Macromolecules*, 53(17):7335–7345, 2020.
 21. Benjamin S Hanson and Lorna Dougan. Intermediate structural hierarchy in biological networks modulates the fractal dimension and force distribution of percolating clusters. *Biomacromolecules*, 22(10):4191–4198, 2021.
 22. Matt D. G. Hughes, Benjamin S. Hanson, Sophie Cussons, Najet Mahmoudi, David J. Brockwell, and Lorna Dougan. Control of nanoscale in situ protein unfolding defines network architecture and mechanics of protein hydrogels. *ACS Nano*, 15(7):11296–11308, July 2021.
 23. Matt D. G. Hughes, Sophie Cussons, Najet Mahmoudi, David J. Brockwell, and Lorna Dougan. Single molecule protein stabilisation translates to macromolecular mechanics of a protein network. *Soft Matter*, 16(27):6389–6399, 2020.
 24. M. Muthukumar. Screening effect on viscoelasticity near the gel point. *Macromolecules*, 22(12):4656–4658, December 1989.
 25. Michael Gasik, Ana Gantar, Saša Novak, et al. Viscoelastic behaviour of hydrogel-based composites for tissue engineering under mechanical load. *Biomedical materials*, 12(2):025004, 2017.
 26. Sabina Improta, Anastasia S Politou, and Annalisa Pastore. Immunoglobulin-like modules from titin i-band: extensible components of muscle elasticity. *Structure*, 4(3):323–337, March 1996.
 27. Robert B Best, Susan B Fowler, Jose L Toca Herrera, Annette Steward, Emanuele Paci, and Jane Clarke. Mechanical unfolding of a titin ig domain: structure of transition state revealed by combining atomic force microscopy, protein engineering and molecular dynamics simulations. *Journal of molecular biology*, 330(4):867–877, 2003.

-
28. Hu Chen, Guohua Yuan, Rickson S Winardhi, Mingxi Yao, Ionel Popa, Julio M Fernandez, and Jie Yan. Dynamics of equilibrium folding and unfolding transitions of titin immunoglobulin domain under constant forces. *Journal of the American Chemical Society*, 137(10):3540–3546, 2015.
 29. Marcelo A Da Silva, Samuel Lenton, Matthew Hughes, David J Brockwell, and Lorna Dougan. Assessing the potential of folded globular polyproteins as hydrogel building blocks. *Biomacromolecules*, 18(2):636–646, 2017.
 30. Vladimir Potapov, Jennifer L. Ong, Rebecca B. Kucera, Bradley W. Langhorst, Katharina Bilotti, John M. Pryor, Eric J. Cantor, Barry Canton, Thomas F. Knight, Thomas C. Evans, and Gregory J. S. Lohman. Comprehensive profiling of four base overhang ligation fidelity by t4 DNA ligase and application to DNA assembly. *ACS Synthetic Biology*, 7(11):2665–2674, October 2018.
 31. Anders Aufderhorst-Roberts, Matt D. G. Hughes, Andrew Hare, David A. Head, Nikil Kapur, David J. Brockwell, and Lorna Dougan. Reaction rate governs the viscoelasticity and nanostructure of folded protein hydrogels. *Biomacromolecules*, 21(10):4253–4260, September 2020.
 32. Jonathan Kaplan, Alessandra Bonfanti, and Alexandre Kabla. RHEOS.jl – a julia package for rheology data analysis. *Journal of Open Source Software*, 4(41):1700, September 2019.
 33. A. Bonfanti, J. L. Kaplan, G. Charras, and A. Kabla. Fractional viscoelastic models for power-law materials. *Soft Matter*, 16(26):6002–6020, 2020.
 34. David A Fancy and Thomas Kodadek. Chemistry for the analysis of protein–protein interactions: rapid and efficient cross-linking triggered by long wavelength light. *Proc. Natl. Acad. Sci. U. S. A.*, 96(11):6020–6024, 1999.
 35. David A Fancy, Carilee Denison, Kyonghee Kim, Yueqing Xie, Terra Holdeman, Frank Amini, and Thomas Kodadek. Scope, limitations and mechanistic aspects of the photo-induced cross-linking of proteins by water-soluble metal complexes. *Chem. Biol. (Oxford, U. K.)*, 7(9):697–708, 2000.
 36. Marcin Wolny, Matthew Batchelor, Peter J. Knight, Emanuele Paci, Lorna Dougan, and Michelle Peckham. Stable single α -helices are constant force springs in proteins. *Journal of Biological Chemistry*, 289(40):27825–27835, October 2014.
 37. Matthew Batchelor, Marcin Wolny, Marta Kurzawa, Lorna Dougan, Peter J. Knight, and Michelle Peckham. Determining stable single alpha helical (SAH) domain properties by circular dichroism and atomic force microscopy. In *Methods in Molecular Biology*, pages 185–211. Springer New York, 2018.
 38. N. Sreerama. Structural composition of betaI- and betaII-proteins. *Protein Science*, 12(2):384–388, February 2003.
 39. Narasimha Sreerama and Robert W Woody. Estimation of protein secondary structure from circular dichroism spectra: comparison of contin, selcon, and cdsstr methods with an expanded reference set. *Analytical biochemistry*, 287(2):252–260, 2000.
 40. S. Aime, L. Cipelletti, and L. Ramos. Power law viscoelasticity of a fractal colloidal gel. *Journal of Rheology*, 62(6):1429–1441, November 2018.

-
41. Mikihiro Takenaka, Toshiaki Kobayashi, Kenji Saijo, Hirokazu Tanaka, Naoki Iwase, Takeji Hashimoto, and Masaoki Takahashi. Comparison in fractal dimension between those obtained from structure factor and viscoelasticity of gel networks of 1, 3:2, 4-bis-o-(p-methylbenzylidene)-d-sorbitol in polystyrene melt at gel point. *The Journal of Chemical Physics*, 121(7):3323–3328, August 2004.
 42. Mohsen Dahesh, Amélie Banc, Agnès Duri, Marie-Hélène Morel, and Laurence Ramos. Spontaneous gelation of wheat gluten proteins in a food grade solvent. *Food Hydrocolloids*, 52:1–10, January 2016.
 43. Takayoshi Matsumoto, Masahiro Kawai, and Toshiro Masuda. Viscoelastic and SAXS investigation of fractal structure near the gel point in alginate aqueous systems. *Macromolecules*, 25(20):5430–5433, September 1992.
 44. P. Patrício, C. R. Leal, J. Duarte, and C. Januário. Rheology of the cytoskeleton as a fractal network. *Physical Review E*, 92(4), October 2015.
 45. MM Ould Eleya, S Ko, and S Gunasekaran. Scaling and fractal analysis of viscoelastic properties of heat-induced protein gels. *Food Hydrocolloids*, 18(2):315–323, 2004.
 46. Michael Helmberger, Michael Pienn, Martin Urschler, Peter Kullnig, Rudolf Stollberger, Gabor Kovacs, Andrea Olschewski, Horst Olschewski, and Zoltán Bálint. Quantification of tortuosity and fractal dimension of the lung vessels in pulmonary hypertension patients. *PLoS ONE*, 9(1):e87515, January 2014.
 47. Aditya Jaishankar and Gareth H McKinley. A fractional k-bkz constitutive formulation for describing the nonlinear rheology of multiscale complex fluids. *Journal of Rheology*, 58(6):1751–1788, 2014.
 48. Paul Duval, Maurine Montagnat, Fanny Grennerat, Jerome Weiss, Jacques Meyssonier, and Armelle Philip. Creep and plasticity of glacier ice: a material science perspective. *Journal of Glaciology*, 56(200):1059–1068, 2010.
 49. Leon G.B. Bremer, Bert H. Bijsterbosch, Robert Schrijvers, Ton van Vliet, and Pieter Walstra. On the fractal nature of the structure of acid casein gels. *Colloids and Surfaces*, 51:159–170, January 1990.
 50. Francois Chambon and H Henning Winter. Linear viscoelasticity at the gel point of a crosslinking pdms with imbalanced stoichiometry. *Journal of Rheology*, 31(8):683–697, 1987.
 51. Kathryn A Whitaker, Zsigmond Varga, Lilian C Hsiao, Michael J Solomon, James W Swan, and Eric M Furst. Colloidal gel elasticity arises from the packing of locally glassy clusters. *Nature communications*, 10(1):1–8, 2019.
 52. H Henning Winter and Francois Chambon. Analysis of linear viscoelasticity of a crosslinking polymer at the gel point. *Journal of rheology*, 30(2):367–382, 1986.
 53. GW Scott Blair, BC Veinoglou, and JE Caffyn. Limitations of the newtonian time scale in relation to non-equilibrium rheological states and a theory of quasi-properties. *Proceedings of the Royal Society of London. Series A. Mathematical and Physical Sciences*, 189(1016):69–87, 1947.
 54. R. C. Koeller. Applications of fractional calculus to the theory of viscoelasticity. *Journal of Applied Mechanics*, 51(2):299–307, June 1984.

-
55. G. W. Scott Blair and F. M. V. Coppen. The subjective conception of the firmness of soft materials. *The American Journal of Psychology*, 55(2):215, April 1942.
 56. Igor M. Sokolov, Joseph Klafter, and Alexander Blumen. Fractional kinetics. *Physics Today*, 55(11):48–54, November 2002.
 57. Ralf Metzler and Joseph Klafter. The random walk's guide to anomalous diffusion: a fractional dynamics approach. *Physics Reports*, 339(1):1–77, December 2000.
 58. M Muthukumar. Dynamics of polymeric fractals. *The Journal of chemical physics*, 83(6):3161–3168, 1985.
 59. T.J. Faber, A. Jaishankar, and G.H. McKinley. Describing the firmness, springiness and rubberiness of food gels using fractional calculus. part i: Theoretical framework. *Food Hydrocolloids*, 62:311–324, January 2017.
 60. H Schiessel, R Metzler, A Blumen, and TF Nonnenmacher. Generalized viscoelastic models: their fractional equations with solutions. *Journal of physics A: Mathematical and General*, 28(23):6567, 1995.
 61. A. J. Holder, N. Badiei, K. Hawkins, C. Wright, P. R. Williams, and D. J. Curtis. Control of collagen gel mechanical properties through manipulation of gelation conditions near the sol–gel transition. *Soft Matter*, 14(4):574–580, 2018.
 62. TA Surguladze. On certain applications of fractional calculus to viscoelasticity. *Journal of Mathematical sciences*, 112(5):4517–4557, 2002.
 63. S. Nicolle, P. Vezin, and J.-F. Paliarne. A strain-hardening bi-power law for the nonlinear behaviour of biological soft tissues. *Journal of Biomechanics*, 43(5):927–932, March 2010.
 64. K. M. Schmoller, P. Fernández, R. C. Arevalo, D. L. Blair, and A. R. Bausch. Cyclic hardening in bundled actin networks. *Nature Communications*, 1(1), December 2010.
 65. Nicholas A. Kurniawan, Bart E. Vos, Andreas Biebricher, Gijs J.L. Wuite, Erwin J.G. Peterman, and Gijsje H. Koenderink. Fibrin networks support recurring mechanical loads by adapting their structure across multiple scales. *Biophysical Journal*, 111(5):1026–1034, September 2016.
 66. Julie Diani, Bruno Fayolle, and Pierre Gilormini. A review on the mullins effect. *European Polymer Journal*, 45(3):601–612, March 2009.
 67. Cornelis Storm, Jennifer J. Pastore, F. C. MacKintosh, T. C. Lubensky, and Paul A. Janmey. Nonlinear elasticity in biological gels. *Nature*, 435(7039):191–194, May 2005.
 68. F. C. MacKintosh, J. Käs, and P. A. Janmey. Elasticity of semiflexible biopolymer networks. *Physical Review Letters*, 75(24):4425–4428, December 1995.
 69. R. Tharmann, M. M. A. E. Claessens, and A. R. Bausch. Viscoelasticity of isotropically cross-linked actin networks. *Physical Review Letters*, 98(8), February 2007.
 70. GangSeob Jung, Zhao Qin, and Markus J. Buehler. Mechanical properties and failure of biopolymers: Atomistic reactions to macroscale response. In *Topics in Current Chemistry*, pages 317–343. Springer International Publishing, 2015.

-
71. Luca Cipelletti, Kirsten Martens, and Laurence Ramos. Microscopic precursors of failure in soft matter. *Soft Matter*, 16(1):82–93, 2020.
 72. Theodor Ackbarow and Markus J. Buehler. Superelasticity, energy dissipation and strain hardening of vimentin coiled-coil intermediate filaments: atomistic and continuum studies. *Journal of Materials Science*, 42(21):8771–8787, July 2007.
 73. Michel Grandbois, Martin Beyer, Matthias Rief, Hauke Clausen-Schaumann, and Hermann E. Gaub. How strong is a covalent bond? *Science*, 283(5408):1727–1730, March 1999.
 74. Ralf Metzler and Joseph Klafter. From stretched exponential to inverse power-law: fractional dynamics, cole–cole relaxation processes, and beyond. *Journal of Non-Crystalline Solids*, 305(1-3):81–87, July 2002.
 75. Hendrik Dietz, Felix Berkemeier, Morten Bertz, and Matthias Rief. Anisotropic deformation response of single protein molecules. *Proceedings of the National Academy of Sciences*, 103(34):12724–12728, August 2006.
 76. Horst Henning Winter and Marian Mours. Rheology of polymers near liquid-solid transitions. In *Neutron Spin Echo Spectroscopy Viscoelasticity Rheology*, pages 165–234. Springer Berlin Heidelberg, 1997.
 77. Ben Fabry, Geoffrey N. Maksym, James P. Butler, Michael Glogauer, Daniel Navajas, and Jeffrey J. Fredberg. Scaling the microrheology of living cells. *Phys. Rev. Lett.*, 87:148102, Sep 2001.
 78. M Kohandel, S Sivaloganathan, G Tenti, and K Darvish. Frequency dependence of complex moduli of brain tissue using a fractional zener model. *Physics in Medicine and Biology*, 50(12):2799–2805, may 2005.
 79. Maarten Jaspers, Matthew Dennison, Mathijs F. J. Mabesoone, Frederick C. MacKintosh, Alan E. Rowan, and Paul H. J. Kouwer. Ultra-responsive soft matter from strain-stiffening hydrogels. *Nature Communications*, 5(1), December 2014.

Acknowledgments: We thank David Head, Ben Hanson, and Matt Hughes for helpful discussions. **Funding:** We gratefully acknowledge funding from the Engineering and Physical Sciences Research Council with grant EP/P02288X/1. The CD spectropolarimeter was funded by the Wellcome Trust with grant WT094232. **Author contributions:** A.A-R, L.D and D.J.B conceived the experiments. A.A-R performed the experiments, analysed the data and wrote the manuscript with contributions from all other authors. S.C expressed and purified proteins. L.D. is the principal investigator and corresponding author. **Competing interests:** The authors declare that they have no competing interests. **Data and materials availability:** All data needed to evaluate the conclusions in the paper are present in the paper and/or the Supplementary Materials.

Supplementary Materials for

Power Law Rheology of Folded Protein Hydrogels

Anders Aufderhorst-Roberts, Sophie Cussons, David J. Brockwell, Lorna
Dougan*

*Corresponding author. Email: l.dougan@leeds.ac.uk

This PDF file includes:

Supplementary Text

Figs. S1 to S12

Supplementary Text

Analysis of Polyprotein Dimensions

The polyprotein structure comprises a concatenated series of five *I27* protein domains as shown in figure S1. Linkers comprising 4-6 amino acids were inserted between domains to decrease inter-domain interactions. A hexahistidine tag is found at the N-terminus and a dicysteine group is found at the C-terminus.

Dimensions and distances are determined using the 'distance' tool in the molecular visualization software PyMOL. The individual *I27* domains each have an N-C end-to-end length of $l_{domain} = 4.66$ nm. Each of the four linker domains contain between 4-6 amino acids with no intrinsic secondary structure. Given that the average linker length is 5 residues, that the average length of an amino acid is 0.35 nm, and assuming that the linker adopts a freely-jointed-chain structure, the total average length of the linker l_{link} is: $l_{link} = 0.35 \text{ nm} \times \sqrt{5} = 0.78$ nm.

From this we may estimate the following:

1. The mean distance between tyrosine crosslink sites is
 $l_{domain} + l_{link} = 5.44$ nm
2. The ratio between the linker length and polyprotein radius as
 $\frac{2l_{link}}{l_{domain}} = 0.34$.



Figure S1. Secondary structure (a) and protein sequence (b) of the *I27*₅ polyprotein used in this study. The molecule comprises five mutated *I27* domains concatenated with unstructured linker regions (light blue). The secondary structure is predominantly composed of β -sheets (rectangles) and contains 5 tyrosine residues, (ringed by purple circles) which act as crosslink sites

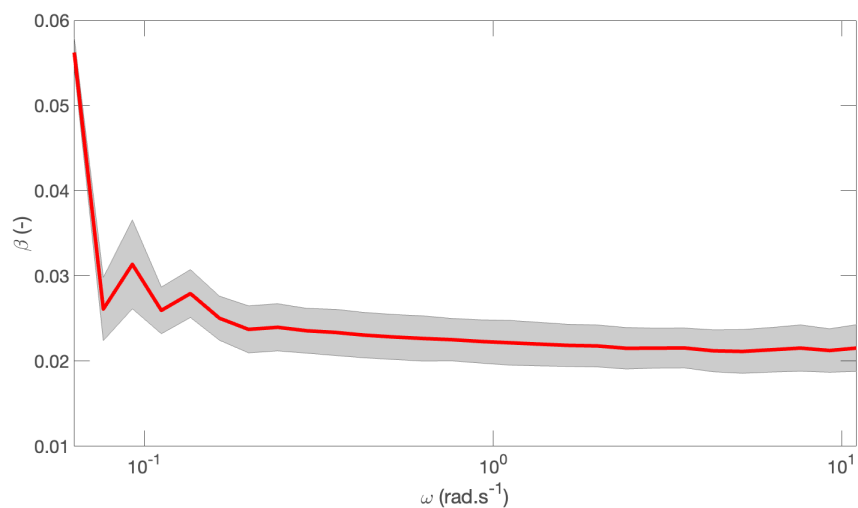


Figure S2. Power law exponent β as verified independently using the Kramers-Kronig relation of G'' and G' . For $\omega > 1 \text{ rad s}^{-1}$, β is shown to plateau to an average value of 0.022 ± 0.002 , in excellent agreement with power laws fitted to G' in figure 1. Error bars (shaded regions) represent averaged measurements.

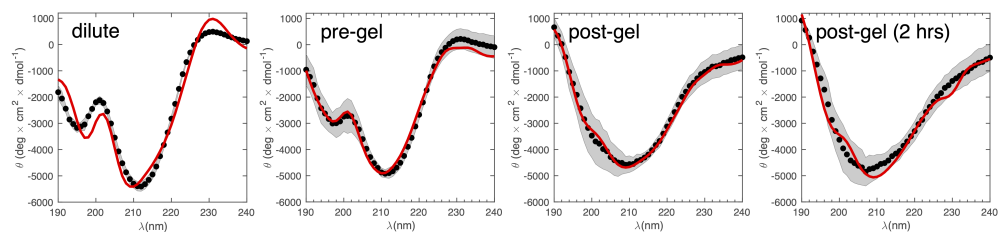
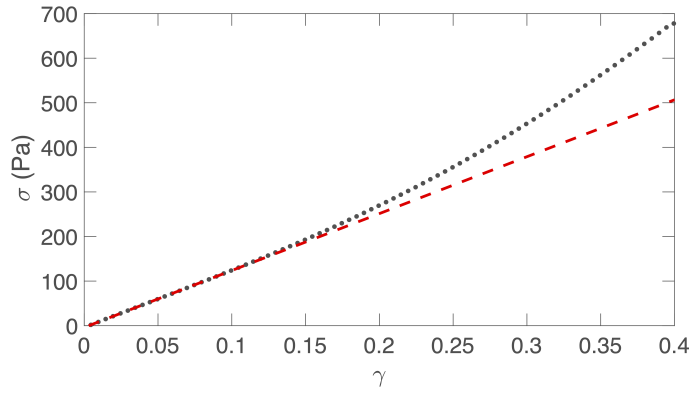


Figure S3. Best fits (solid red lines) to the mean residue ellipticity of $I27_5$ hydrogels (black circles) at dilute concentrations ($5 \mu\text{M}$) and at each stage of the gelation process. Fits are carried using the CONTINLL parameter set in Dichroweb. Error bars (shaded regions) represent averaged measurements across different samples.



4
Figure S4. Representative stress-strain Curve of an $I27_5$ hydrogel, captured at a shear strain rate of 0.01 s^{-1} (black dotted line). Excellent agreement with a linear viscoelastic response (red dashed line) is observed for strain $\gamma < 0.1$.

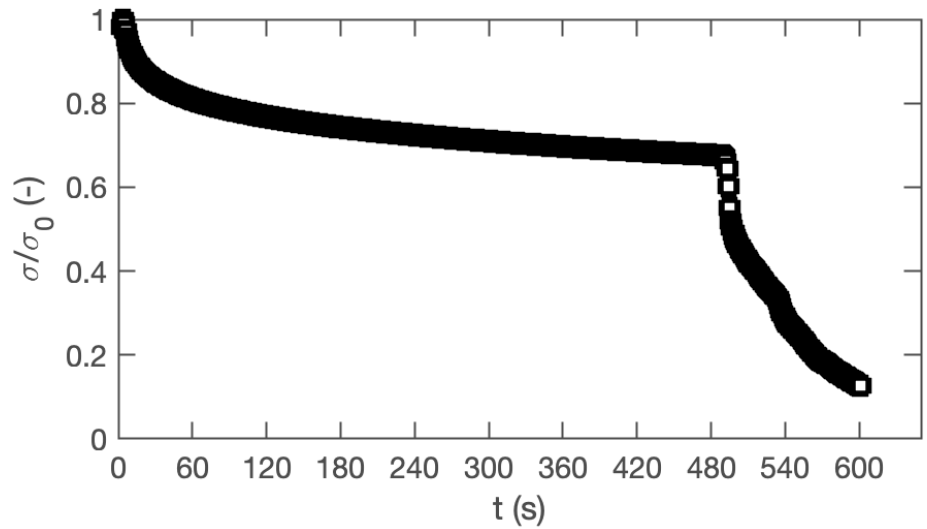


Figure S5. Representative stress relaxation curve at high step strain ($\gamma = 0.35$). The relaxation curve is discontinuous, indicating that the sample undergoes irreversible fracture.

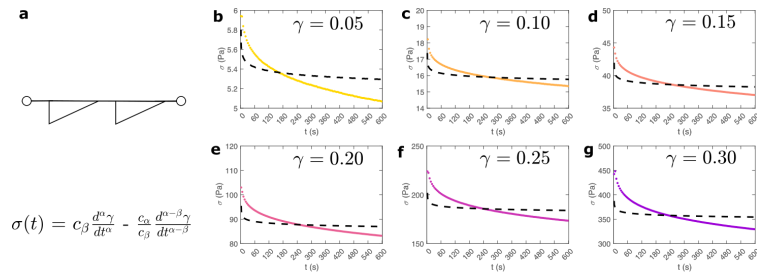


Figure S6. Best fit of a fractional Maxwell model (a) to stress relaxation data at a range of different applied strains. Model fits are shown as dashed lines.

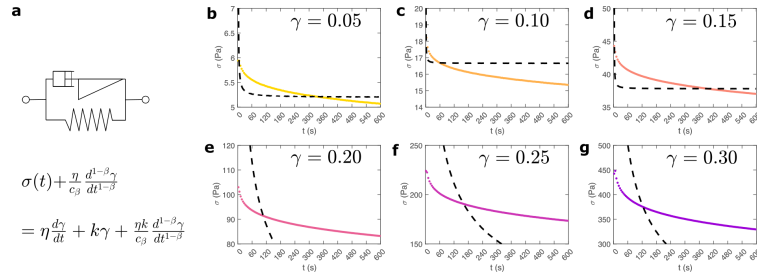


Figure S7. Best fit of a modified Fractional viscoelastic model comprising a fractional springpot element in series with a spring and in parallel with a dashpot (a). The fit is applied to stress relaxation data at a range of different applied strains (b)-(g). Model fits are shown as dashed lines.

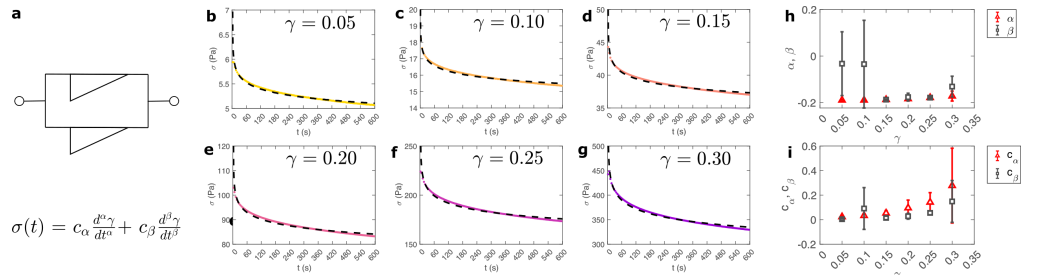


Figure S8. Best fit of a fractional Kelvin Voigt model comprising two springpot elements in parallel. (a). The fit is applied to stress relaxation data at a range of different applied strains (b)-(g). While the model fits the data closely, the parameters c_α and α are within the error margins of parameters c_β and β (h)-(i) suggesting that additional parameters cause the fitting to become degenerate. Error bars represent averaged measurements across different samples. Model fits are shown as dashed lines.

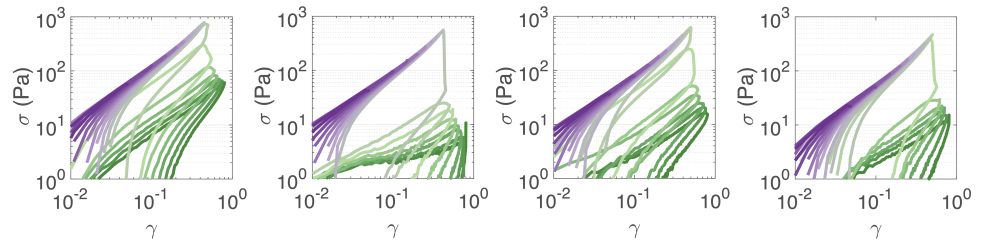


Figure S9. Representative cyclic loading data showing measured stress with respect to applied strain. Solid lines are loading curves, dashed lines are unloading curves. Colours indicate different loading cycles. Repeat measurements show largely identical nonlinear response, with only slight differences in the network fracture point, denoted by a sudden decrease in stress.

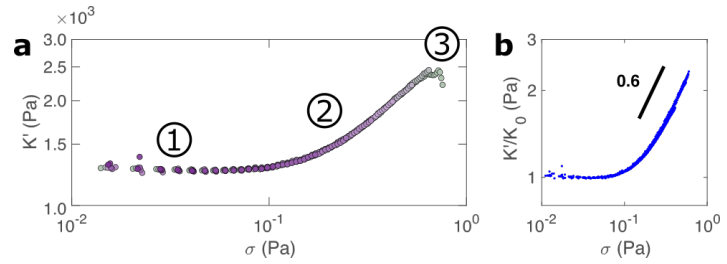


Figure S10. Differential elastic modulus K' with respect to the sample stress, extracted from multiple loading cycles (a). Colours and regimes of mechanical response (1-3) are equivalent to figure 4. Once K' is normalised to account for slight differences in the linear modulus G_0 , data from all repeat measurements superimpose perfectly on to a single curve (b). The hydrogel stiffens as $K' \sim \sigma^{0.6}$.

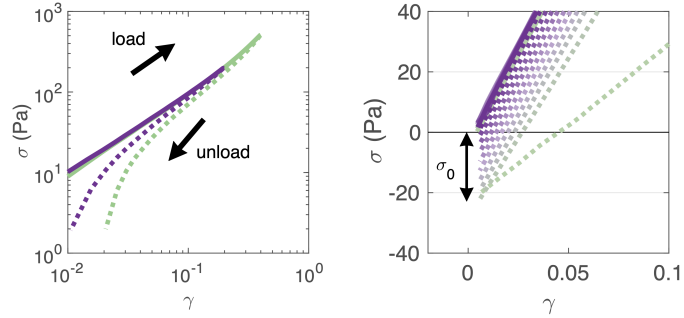


Figure S11. Definition of the remodelling parameter σ_0 . As the network is progressively remodelled after repeated loading cycles, a negative stress σ_0 required to return the network to zero strain. An increase in σ_0 indicates an increase in network remodelling.

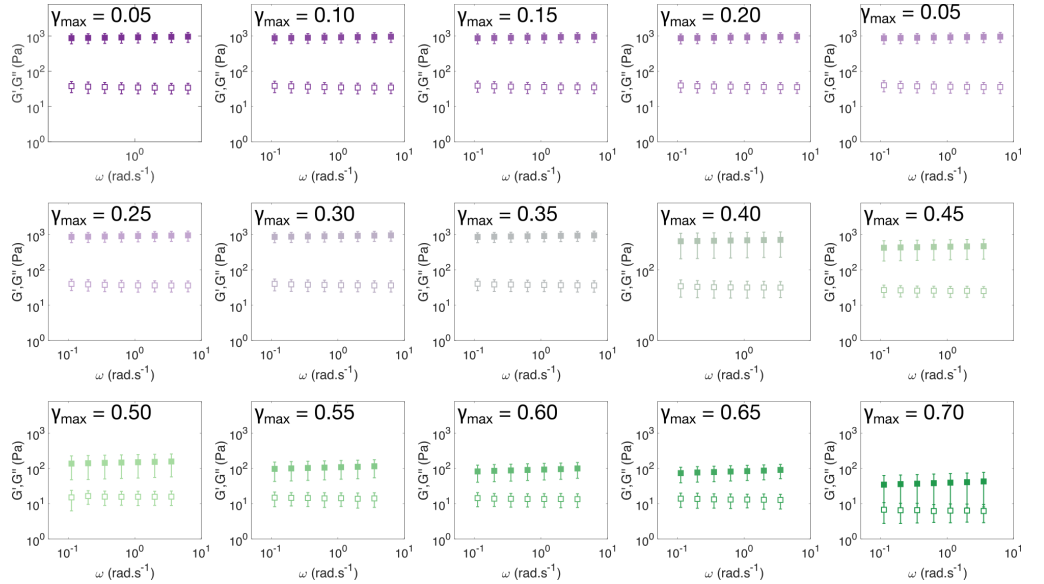


Figure S12. Representative frequency sweeps of the $I27_5$ hydrogels following the application of triangular strain pulses of increasing magnitude. Each frequency sweep probes the linear viscoelastic properties of the hydrogel after deformation. The spectra remain remarkably consistent at applied strains γ below approximately 0.4, at which point the network undergoes irreversible fracture